Progress In Electromagnetics Research, Vol. 144, 115–122, 2014

Octave Division Motion Compensation Algorithm for Near-Range Wide-Beam SAR Applications

Huaming Wu* **and Thomas Zwick**

Abstract—The space-variant motion errors are specific to different targets and proportional to the beamwidth of a synthetic aperture radar (SAR) system, which makes them very difficult to be compensated for a SAR system with wide beamwidth. In this paper, a motion compensation (MoCo) algorithm that exploits the features of the geometry of near-range SAR applications is proposed. By dividing the whole range swath into several octave sub-swaths, the effects of space-variant motion errors can be greatly reduced, especially for targets at nearer range, with low computational load.

1. INTRODUCTION

Synthetic aperture radar (SAR) systems have been used for remote sensing applications for the last several decades [1]. The effects of motion errors and the corresponding solutions have also been studied extensively almost since SAR's debut in 1950s [2]. In the last decade, the development of low-cost radar systems has led to the hope that SAR systems might be used for civil near-range applications, e.g., parking lot detection [3]. However, motion compensation (MoCo) continues to be a challenging problem in this field.

Motions errors result from differences between the real and the nominal trajectory of a radar sensor, and they result in distortions in the final SAR image. For the ease of explanation, a constant deviation from the nominal trajectory in y axis in the 2D xy-plane and different components of the motion errors of a certain target t are illustrated in Figure 1. On the left side of Figure 1, the distance between the target and the radar's nominal position, r_t, is denoted by green color, while the real distance between the target and the radar's real position, $\tilde{r}_t$, is denoted by red color. The difference between $\tilde{r}_t$ and r_t is the target's motion error, Δr_t, which is denoted by lilac color. As depicted on the right side of Figure 1, Δr_t can be decomposed into two components, i.e., $\Delta r_t = \Delta r_{\text{in}} + \Delta r_{\text{var}}$. The space-invariant motion error, Δr_{in}, is the difference between the real trajectory and the nominal trajectory, which is denoted by the blue line. The space-variant motion error, Δr_{var}, is the residual part of Δr_t, which is denoted by the lilac dash line. It can be seen that Δr_t, which is denoted by the lilac solid line, is not linear even when the real trajectory is linear.

For SAR systems of narrow antenna beamwidth, Ψ, e.g., $\Psi < 10^\circ$ in remote sensing SAR operating at C or X frequency band, Δr_{var} can be ignored [4]. The so-called first-order MoCo can be performed by multiplying the raw SAR data with a compensation phase term built with the knowledge of Δr_{in}. However, since Δr_{var} increases with Ψ at the edge of the synthetic aperture, it becomes non-negligible when Ψ is larger than a certain value. For instance, Ψ can be larger than 30° in a SAR system working at VHF/UHF band [5]. Moreover, Ψ can easily be larger than 60° for a near-range SAR system which intends to take advantage of the already existing automotive radar [6].

For remote sensing SAR applications working in stripmap mode, normal SAR algorithms have been modified to address the problems caused by the high dynamics of an airplane. To compensate azimuth-variant motion errors in the case of wide Ψ, at least 4 types of MoCo algorithms have been

Received 8 November 2013, Accepted 18 December 2013, Scheduled 20 December 2013

* Corresponding author: Huaming Wu (huaming.w@gmail.com).

The authors are with the Institut fuer Hochfrequenztechnik und Elektronik, Karlsruhe Institute of Technology, Geb. 30.10, Kaiserstr 12, Karlsruhe 76128, Germany.

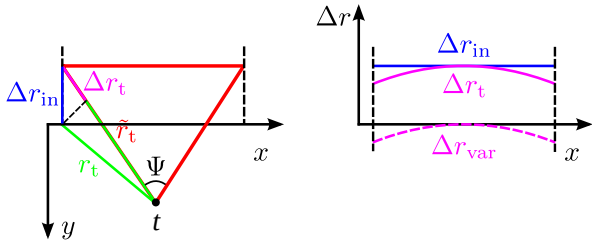

Figure 1. The relationship between Δr_t, Δr_{in} and Δr_{var}.

proposed [7–10]. However, the MoCo algorithms proposed in [7–9] all make a compromise among computational load, angle accommodation and trajectory deviation accommodation. Alternatively, the MoCo algorithm proposed in [10] trades the computational load for processing quality. For each pixel (target) the information of its precise topography is needed. In addition, a pair of extra azimuth Fourier and inverse Fourier transforms of the whole processing block where the pixel is within is performed. Therefore, such pixel-wise algorithm is still impracticable for real-time civil applications given the performance of a realistic hardware environment and the lack of topography information.

For near-range SAR systems of wide Ψ, performing alone the first-order MoCo may introduce a worse extra space-variant motion error component into the signals of targets at nearer range. This effect is introduced in Section 2, where the properties of the so-called artificial motion errors are analyzed geometrically and mathematically. Accordingly, in Section 3, a new MoCo algorithm called octave division algorithm (ODA) for stripmap mode SAR is proposed. Subsequently, the algorithm is verified by a SAR simulator programmed in MATLAB in Section 4.

2. ARTIFICIAL MOTION ERROR

Generally, the nominal trajectory for SAR processing of a whole scene is defined as the optimal straight-line path that results in the minimal root-mean-square (RMS) of the difference between the optimal straight-line path and the real trajectory. However, for each target within the scene, in terms of resulting in minimal RMS of Δr_{in}, the optimal straight-line path within its own synthetic aperture could be variant. For example, quadratic or higher-order motion components are defined as Δr_{in} with regard to a long optimal straight-line path within the synthetic aperture of a further target. However, parts of these Δr_{in} within the shorter synthetic apertures of a nearer target can be just linear, as long as the target is close enough to the real trajectory. They would not exist if the optimal straight-line path was defined with respect to the nearer target. In this paper, such linear motion errors are defined as artificial motion errors for targets at nearer range.

Since artificial motion errors arise from the differences between optimal straight-line paths with regard to targets at different ranges, they are more severe in near-range applications than in remote sensing applications. Specifically, two types of deteriorations resulting from artificial motion errors are discussed as follows.

The first type of resulting deterioration is the loss of relative position information. As shown in Figure 2, the same target's position in the final SAR image with and without a complete MoCo has been illustrated in the left and right side respectively. As illustrated in the left figure, the xy-coordinate system is dictated by the optimal straight-line path with respect to further targets, i.e., the x axis. In this case, the real trajectory within the synthetic aperture of target t (the gray part of the real trajectory), though is a straight line, is considered containing linear motion errors. If the length of the SAR processing block, L, reduces to that of the synthetic aperture length of target t, L_t, the real trajectory will overlap with the optimal straight-line path with respect to target t, i.e., the x' axis, in the $x'y'$-coordinate system. In this case, the motion errors reduce to zero. Without MoCo, the range of the closest approach of target t, $r'_{t,0}$, can be correctly obtained in the $x'y'$-coordinate system. On the other hand, with MoCo for Δr_{in} in the xy-coordinate system, an incorrect range of the closest approach, $r_{t,0}$, is obtained.

The second type of deterioration caused by artificial motion errors is equivalent to that caused by

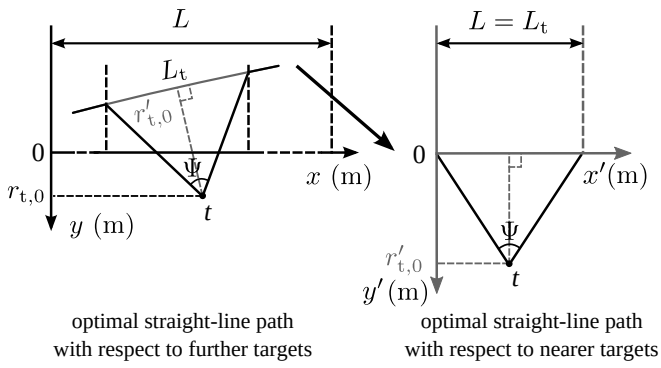

Figure 2. The loss of relative position information caused by artificial motion errors.

quadratic or higher-order motion errors, when only the first-order MoCo is applied. Mathematically, the first-order MoCo can be expressed as

$$\tilde{s}_{\mathrm{IF,in}}\left(x_{\mathrm{am}}, k_r\right) = \tilde{s}_{\mathrm{IF}}\left(x_{\mathrm{am}}, k_r\right) \cdot \exp\left(jk_r \Delta r_{\mathrm{in}}\right) = s_{\mathrm{IF}}\left(x_{\mathrm{am}}, k_r\right) \cdot \exp\left(-jk_r \Delta r_{\mathrm{var}}\right). \tag{1}$$

In (1), $\tilde{s}_{\mathrm{IF}}(x_{\mathrm{am}}, k_r)$ is the raw SAR IF signal in the azimuth-time domain, x_{am}, and range-frequency domain, k_r, with motion errors, Δr_t; $s_{\mathrm{IF}}(x_{\mathrm{am}}, k_r)$ is the ideal SAR signal without motion error; $\tilde{s}_{\mathrm{IF,in}}(x_{\mathrm{am}}, k_r)$ is the SAR signal after performing the first-order MoCo, which now contains the extra space-variant motion errors, Δr_{var}. If an antenna with wide Ψ is used and no further MoCo is applied, Δr_{var} in $\tilde{s}_{\mathrm{IF,in}}(x_{\mathrm{am}}, k_r)$ can be substantial at the edge of synthetic aperture, both in near-range applications and remote sensing applications.

As mentioned in the first paragraph of this section, in near-range applications, the linear component of Δr_{in}, i.e., artificial motion errors, for a certain nearer target would not be existing if the an optimal straight-line path was defined with respect to this specific target. Therefore, by ignoring artificial motion errors, the first-order MoCo is essentially performed with respect to the specific optimal straight-line path for the nearer target. Correspondingly, the artificial-motion-errors-resultant Δr_{var} reduce to zero. As a result, the deterioration caused by the residual Δr_{var} in (1) can be greatly reduced.

3. OCTAVE DIVISION ALGORITHM

A MoCo algorithm is proposed to divide the whole range swath into several sub-swaths to reduce the differences between optimal straight-line paths with respect to different targets within the same processing block. Consequently, artificial motion errors within each sub-swaths can be reduced. According to the mechanism of dividing the range swath, the algorithm is called octave division algorithm (ODA). Assuming the motion data of the radar sensors are correctly obtained, the block diagram of ODA is illustrated in Figure 3.

For a FMCW radar scheme, after dechirp-on-receive processing, the raw SAR IF signal deteriorated by motion errors, $\tilde{s}_{\mathrm{IF}}$, are in the azimuth-time range-frequency domain. First of all, $\tilde{s}_{\mathrm{IF}}$ is sampled by an ADC in the range frequency domain. The sampling frequency, f_{s}, should meet the Nyquist criterion, i.e., $f_{\mathrm{s}} > 2f_{\tilde{s}_{\mathrm{IF}},\,\mathrm{max}}$. Since $f_{\tilde{s}_{\mathrm{IF}},\,\mathrm{max}}$ is the maximum frequency of $\tilde{s}_{\mathrm{IF}}$, it can be calculated by differentiating the IF signal's phase with respect to t as

$$\begin{aligned} f_{\tilde{s}_{\mathrm{IF}},\,\mathrm{max}} &= \max\left\{\frac{d}{dt}\left[\frac{2}{c}\left(f_{\min} + \gamma\hat{t}\right)\tilde{r}_t\right]\right\} = \frac{2}{c} \cdot \max\left[\gamma \cdot \tilde{r}_t \cdot \frac{d\hat{t}}{dt} + \left(f_{\min} + \gamma\hat{t}\right) \cdot \frac{d\tilde{r}_t}{dt}\right] \\ &= \frac{2}{c} \cdot \left[\gamma \cdot y_{\mathrm{SC}} + f_{\max} \cdot v \cdot \sin\left(\frac{\Psi}{2}\right)\right]. \end{aligned} \tag{2}$$

In (2), $f_{\min}$ is the minimum frequency of the transmitted chirp, γ the chirp rate, v the radar's velocity, and y_{SC} the maximum range of the scene. The first term in the square brackets denotes the position information and the second term denotes the velocity information. It is clear that the sampling frequency, f_s, in the range-frequency domain is proportional to y_{SC}.

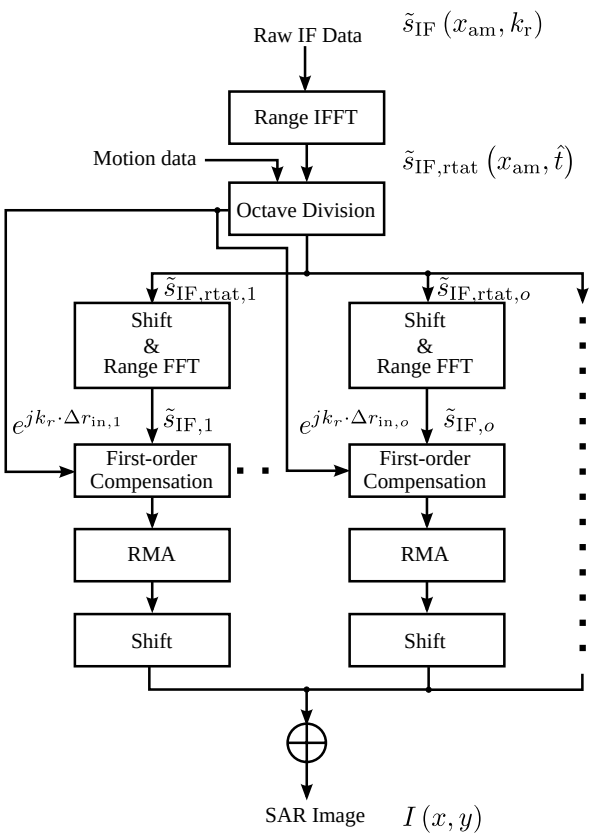

Figure 3. Block diagram of ODA.

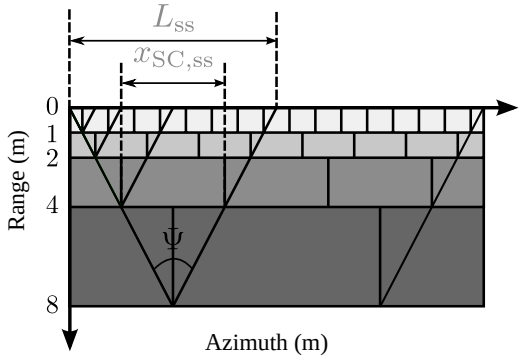

Figure 4. Octave division in data space $\tilde{s}_{\mathrm{IF,rtat}}(x_{\mathrm{am}}, \hat{t})$, where L_{ss} and $x_{\mathrm{SC,ss}}$ of sub-swath of $y \in [2,\ 4]$ m are denoted.

After sampling, the digital $\tilde{s}_{\mathrm{IF}}$ signal is transferred from azimuth-time range-frequency domain, $\tilde{s}_{\mathrm{IF}}(x_{\mathrm{am}}, k_r)$, to azimuth-time range-time domain, $\tilde{s}_{\mathrm{IF,rtat}}(x_{\mathrm{am}}, \hat{t})$, via performing a range IFFT.

Then, as illustrated in Figure 4, the data space of $\tilde{s}_{\mathrm{IF,rtat}}(x_{\mathrm{am}}, \hat{t})$ is divided into several overlapped segments both in azimuth and range directions. The signal of each segment is represented by $\tilde{s}_{\mathrm{IF,rtat},o}$ with subscript "o" denoting the corresponding index.

The next step is to transfer each segment back to the azimuth-time range-frequency domain. By shifting each $\tilde{s}_{\mathrm{IF,rtat},o}$ to range zero, the maximum range of each segment is reduced to its length in range direction. According to (2), the maximum frequency of the range frequency of each segment, $f_{\tilde{s}_{\mathrm{IF,rtat},o,\,\max}}$, is reduced too. Therefore, performing a range FFT on each segment with a shorten number of samples corresponding to the segment's length will not cause aliasing in the range-frequency domain.

To perform a first-order MoCo, each $\tilde{s}_{\mathrm{IF},o}$ is multiplied with a corresponding MoCo phase term, $\exp(jk_r \cdot \Delta r_{\mathrm{in},o})$. Here, the optimal straight-line path for each segment is obtained by performing linear fitting on the corresponding motion data. As will be explained later, the mechanism of octave division guarantees that most of the artificial motion errors will be excluded from $\Delta r_{\mathrm{in},o}$.

Subsequently, each segment data are processed using range migration algorithm (RMA) [1]. In the end, the result of each segment is shifted both in range and azimuth directions and then stitched back to form the final SAR image.

The mechanism of octave division is explained in the following paragraphs.

First of all, a parameter, *MSR*, has been defined to classify motion components. *MSR* is the motion frequency to synthetic aperture frequency ratio, which is similar to the one defined in [1] and can be expressed as

$$MSR = \frac{f_m}{f_{\mathrm{syn}}} = \frac{L_t}{\frac{v}{f_m}} = \begin{cases} [0,\ 0.25] & \text{Linear} \\ [0.25,\ 0.75] & \text{Quadratic} \\ [0.75,\ \infty] & \text{Sinusoidal} \end{cases}. \tag{3}$$

In (3), f_m is the frequency of the motion components within the target's synthetic aperture; f_{syn} is the synthetic aperture frequency, which is the reciprocal of synthetic aperture time, $\frac{L_t}{v}$; L_t is the target's synthetic aperture length, which can be calculated by

$$L_t = 2 \cdot r_{t,0} \cdot \tan\left(\frac{\Psi}{2}\right). \tag{4}$$

Note that the term $^{v}/_{f_m}$ is the period of the motion error in unit of m, and therefore *MSR* is also the ratio between the target's synthetic aperture length and the motion component's period.

For any motion components, when their MSR with respect to the nearest targets are smaller than 0.25, they are considered to be linear. In this case, the optimal straight-line path should almost overlap with such motion components. However, as (3) and (4) indicate, *MSR* is proportional to target's range. For the same motion errors, their *MSR* with respect to the furthest targets could become larger than 0.25. Consequently, the resultant optimal straight-line path will not overlap with the one obtained with respect to the nearest targets. As a result, artificial motion errors are introduced for the nearer range targets.

As the discussion above attests, artificial motion errors cannot be completely avoided. However, they can be suppressed to a certain degree by restricting the ratio between the furthest range and the nearest range of a SAR processing segment, which can be expressed as

$$FNR = \frac{r_{t,0,\mathrm{Furthest}}}{r_{t,0,\mathrm{Nearest}}}. \tag{5}$$

By substituting (3) and (4) into (5), *FNR* can be expressed as the ratio of the MSR with respect to the furthest target to that with respect to the nearest target as

$$FNR = \frac{\dfrac{2 \cdot r_{t,0,\mathrm{Furthest}} \cdot \tan\left(\dfrac{\Psi}{2}\right)}{\dfrac{v}{f_m}}}{\dfrac{2 \cdot r_{t,0,\mathrm{Nearest}} \cdot \tan\left(\dfrac{\Psi}{2}\right)}{\dfrac{v}{f_m}}} = \frac{MSR_{\mathrm{Furthest}}}{MSR_{\mathrm{Nearest}}}. \tag{6}$$

Here we assume the effects of the residual artificial motion errors can be ignored for the nearer range targets, if for any motion component when MSR_{Nearest} is 0.25 (as the upper limit of the linear region), MSR_{Furthest} is smaller than 0.5 (as the middle value of the quadratic region). In such case, any linear motion component within the synthetic aperture of the nearest target will approximately not be part of the motion errors that need to be compensated for the furthest target. Therefore the upper limit of *FNR* can be determined as

$$FNR = \frac{MSR_{\mathrm{Furthest}}}{MSR_{\mathrm{Nearest}}} < \frac{0.5}{0.25} = 2. \tag{7}$$

Subsequently, by analogy with the octave frequency definition in the sound processing field, the whole range swath can be divided into several octave sub-swaths, i.e., the whole range swath is divided at $y = 1$, 2, 4, 8 and 16 m as illustrated in Figure 4.

As a trade-off between processing efficiency and accommodation of artificial motion errors, for each range sub-swath the imaged scene along azimuth direction is divided into equal segments with the length of $x_{\mathrm{SC,ss}} = 2 \cdot r_{t,0,\mathrm{Furthest,ss}} \cdot \tan(\frac{\Psi}{2})$, where subscript "ss" denotes sub-swath. As illustrated in Figure 4, the corresponding data segment length can be calculated as $L_{\mathrm{ss}} = 2x_{\mathrm{SC,ss}}$, and the overlapping length of segment along azimuth direction is $x_{\mathrm{SC,ss}}$.

Compared with the spotlike algorithm proposed in [7], the extra computation load of ODA comes from the extra range IFFT and range FFT. According to the SAR algorithm computation load analysis presented in [11], the computation load of the ODA is about 46% higher than that of the spotlike algorithm. Furthermore, the other two algorithms proposed in [8, 9] perform extra azimuth Fourier transforms, which generally have higher computation load than range Fourier transforms in near-range SAR applications. Therefore, ODA has less computation load than the other three MoCo algorithms [8–10].

It should be noted that the artificial motion errors are exclusive to near-range SAR applications. The range swath of SAR system in near-range applications is

$$\frac{2D^2}{\lambda_{\min}} < r_{t,0} < r_{\max}. \tag{8}$$

Here, $\frac{2D^2}{\lambda_{\min}}$ is the far-field boundary of the antenna as defined in [12], where D ($D > \lambda_{\max}$) is the maximum overall dimension of antenna and $\lambda_{\min}$ the minimum wavelength of the transmitted chirp; $r_{\max}$ is the maximum working range of the SAR system. For example, by applying $D = 4.2$ cm, $\lambda_{\min} = 1.28$ cm and $r_{\max} = 18$ m, the number of octave sub-swaths can be calculated as

$$N_{\text{sub-swath}} = \log_2(FNR) = \log_2\left(\frac{r_{\max}}{\frac{2D^2}{\lambda_{\min}}}\right) \approx 6. \tag{9}$$

As a contrast, in remote sensing SAR application, *FNR* is usually smaller than 2. For instance, the airborne P-3 SAR used for detection of concealed targets under foliage images the scene with range swath of [5387.5, 6354.9] m [13]. The corresponding *FNR* is about 1.2, which means that motion errors have almost the same *MSR* for all the targets within the whole range swath. Therefore it is unsuitable to apply ODA in remote sensing applications.

4. VERIFICATION

To demonstrate the effects of artificial motion errors and verify the proposed ODA, a scene including a point target at nearer range ($y_t = 0.5$ m) and a point target at further range ($y_t = 3.5$ m) has been simulated. As shown in Figure 5(a), the real trajectory depicted in the xy-coordinate system consists of two components: a sinusoidal component and a linear component. As discussed in Section 2, the linear component is part of motion errors that are determined with regard to targets at furthest range. Four MoCo strategies have been applied, and the corresponding SAR images of the two point targets are shown in Figure 5(b). The broadening factor of azimuth resolution, F_B, is defined as the ratio of the real azimuth resolution (with motion errors) to the ideal azimuth resolution (without motion errors).

In accordance with the analysis in Section 2 that the target at nearer range suffers most from the artificial motion error, a more concentrated image of the target at nearer range can be obtained without MoCo than with the first-order MoCo. Moreover, both targets images in the case of the first-order MoCo are deteriorated by the artificial motion errors that are determined with regard to targets at furthest range.

Since the spotlike MoCo is tuned to concentrate the further target with $y_t = 3.5$ m, the further target at the center of the processed block has perfect concentration. However, the nearer target away from the center area suffers more residual motion errors than in the case of the first-order MoCo. As a contrast, the ODA removes completely the artificial motion errors, thereby having the best performance

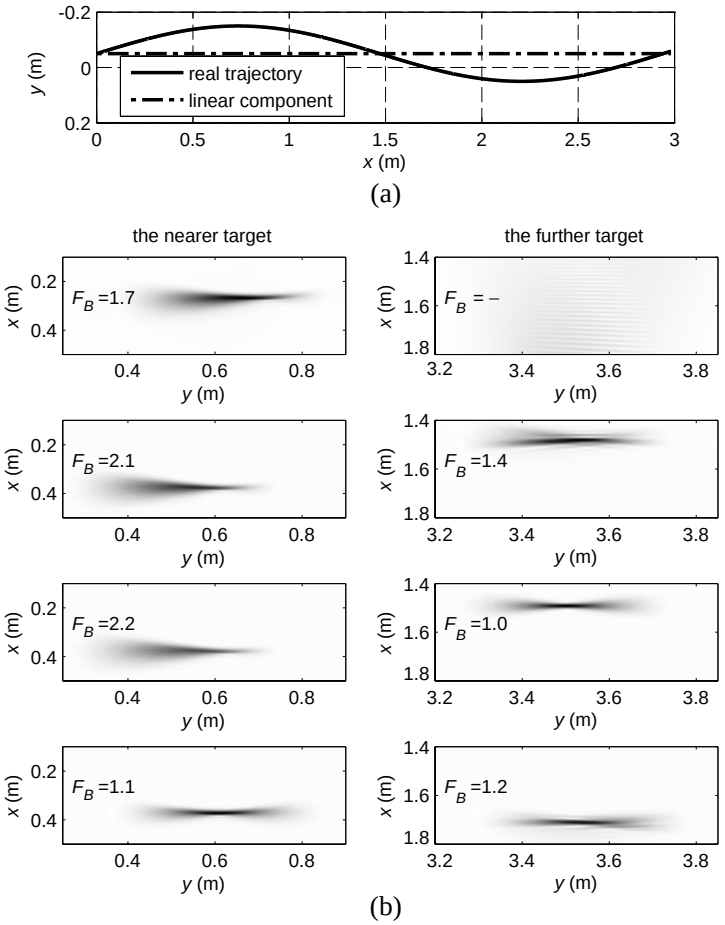

Figure 5. Comparison of different MoCo strategies (system parameters: center frequency $f_c = 24\,\text{GHz}$, transmission bandwidth $B = 1\,\text{GHz}$, $\Psi = 40°$): (a) the trajectory in the long-term nominal coordinate system; (b) normalized SAR images: left column shows the target at nearer range ($y_t = 0.5\,\text{m}$), right column shows the target at further range ($y_t = 3.5\,\text{m}$); the MoCo strategies are shown from up to down in the following order: without MoCo, with first-order MoCo, with spotlike MoCo and with ODA MoCo; the broadening factors of azimuth resolution, F_B, are labeled.

for the nearer target. The residual broadening effects after MoCo are caused by residual azimuth-variant motion errors. Although they can be compensated by the algorithms proposed in [8–10], a much higher computation load would result.

5. CONCLUSION

For near-range applications, due to the high ratio of the furthest range to the nearest range, *FNR*, a SAR system with wide Ψ will suffer from a special type of motion error. The so-called artificial motion errors arise from the differences between the optimal straight-line paths for targets at different ranges. They are introduced especially for the nearer range targets after a common first-order MoCo is performed, and are proportional to the *FNR* of a SAR processing block.

Although artificial motion errors are unavoidable, the proposed ODA is designed to suppress them to a certain degree. The ODA divides the whole SAR scene into sub-swaths, thereby reducing the *FNR* of each sub-swath. At the cost of about 46% extra computation load, the ODA can improve the azimuth resolution by 100% for near range targets compared to the spotlike MoCo algorithm. On the other hand, the ODA has better performance for near-range applications in terms of computational load than the other MoCo algorithms designed for remote sensing applications.

REFERENCES

1. Carrara, W. G., R. M. Majewski, and R. S. Goodman, *Spotlight Synthetic Aperture Radar: Signal Processing Algorithms,* Artech House, 1995.
2. Mims, J. H. and J. L. Farrell, "Synthetic aperture imaging with maneuvers," *IEEE Transactions on Aerospace and Electronic Systems*, Vol. 4, No. 4, 410–418, 1972.
3. Wu, H. and T. Zwick, "Automotive SAR for parking lot detection," *Proc. of German Microwave Conference, GeMiC 2009*, 1–8, 2009.
4. Moreira, A. and Y. Huang, "Airborne SAR processing of highly squinted data using a chirp scaling approach with integrated motion compensation," *IEEE Transactions on Geoscience and Remote Sensing*, Vol. 32, No. 5, 1029–1040, 1994.
5. Goodman, R., S. Tummala, and W. Carrara, "Issues in ultra-wideband, widebeam SAR image formation," *Record of the IEEE 1995 International Radar Conference*, 479–485, 1995.
6. Dominik, H., "Short range radar — Status of UWB sensors and their applications," *Proc. European Radar Conference, EuRAD 2007*, 251–254, 2007.
7. Carrara, W. G., "Motion compensation algorithm for widebeam stripmap SAR," *Proc. of SPIE*, Vol. 2487, 13–23, 1995.
8. Potsis, A., A. Reigber, J. Mittermayer, A. Moreira, and N. Uzunoglou, "Sub-aperture algorithm for motion compensation improvement in wide-beam SAR data processing," *Electronics Letters*, Vol. 37, No. 23, 1405–1407, 2001.
9. Zheng, X., W. Yu, and Z. Li, "Motion compensation for widebeam SAR based on frequency division," *Journal of Electronics (China)*, Vol. 25, No. 5, 607–615, 2008.
10. DeMacedo, K. A. C. and R. Scheiber, "Precise topography- and aperture-dependent motion compensation for airborne SAR," *IEEE Geoscience and Remote Sensing Letters*, Vol. 2, No. 2, 172–176, 2005.
11. Cumming, I. G. and F. H. Wong, *Digital Processing of Synthetic Aperture Radar Data: Algorithms and Implementation*, Artech House, 2005.
12. Balanis, C. A., *Antenna Theory: Analysis and Design,* 2nd Edition, Wiley-Interscience, 2007.
13. Soumekh, M., D. Nobles, M. Wicks, and G. Genello, "Signal processing of wide bandwidth and wide beamwidth P-3 SAR data," *IEEE Transactions on Aerospace and Electronic Systems*, Vol. 37, No. 4, 1122–1141, 2001.